Base-enhanced catalytic water oxidation by a carboxylate–bipyridine Ru(II) complex

Na Song, Javier J. Concepcion[1], Robert A. Binstead, Jennifer A. Rudd, Aaron K. Vannucci[2], Christopher J. Dares, Michael K. Coggins, and Thomas J. Meyer[3]

Department of Chemistry, University of North Carolina at Chapel Hill, Chapel Hill, NC 27599-3290

Contributed by Thomas J. Meyer, March 9, 2015 (sent for review January 6, 2015; reviewed by Randolph Thummel)

In aqueous solution above pH 2.4 with 4% (vol/vol) CH_3CN, the complex $[Ru^{II}(bda)(isoq)_2]$ (bda is 2,2′-bipyridine-6,6′-dicarboxylate; isoq is isoquinoline) exists as the open-arm chelate, $[Ru^{II}(CO_2\text{-bpy-}CO_2^-)(isoq)_2(NCCH_3)]$, as shown by ^1H and ^{13}C-NMR, X-ray crystallography, and pH titrations. Rates of water oxidation with the open-arm chelate are remarkably enhanced by added proton acceptor bases, as measured by cyclic voltammetry (CV). In 1.0 M PO_4^{3-}, the calculated half-time for water oxidation is ∼7 μs. The key to the rate accelerations with added bases is direct involvement of the buffer base in either atom–proton transfer (APT) or concerted electron–proton transfer (EPT) pathways.

water oxidation catalysis | Ru polypyridyl complexes | electrocatalysis | solar energy | water splitting

Metal-complex catalyzed water oxidation continues to evolve with new catalysts and new mechanistic insights (1–9). Studies on single-site Ru catalysts such as $[Ru^{II}(Mebimpy)(bpy)(OH_2)]^{2+}$ [Mebimpy is 2,6-bis(1-methylbenzimidazol-2-yl)pyridine; bpy is 2,2′-bipyridine; Fig. 1], both in solution and on surfaces, reveal mechanisms in which stepwise oxidative activation of aqua precursors to Ru^V=O is followed by rate-limiting O–O bond formation (10–15). The results of kinetic and mechanistic studies have revealed the importance of concerted atom–proton transfer (APT) in the O–O bond-forming step. In APT, the O–O bond forms in concert with H^+ transfer to water or to an added base (11, 12, 16–19). APT can promote dramatic rate enhancements. In a recent study on surface-bound $[Ru(Mebimpy)(4,4'\text{-}((HO)_2OPCH_2)_2bpy)(OH_2)]^{2+}$ [4,4′-((HO)$_2$OPCH$_2$)$_2$bpy is 4,4′-bis-methlylenephosphonato-2,2′-bipyridine] stabilized by atomic layer deposition, a rate enhancement of $\sim 10^6$ was observed with 0.012 M added PO_4^{3-} at pH 12 compared with oxidation at pH 1 (20).

Sun and coworkers (21, 22) have described the Ru single-site water oxidation catalysts, $[Ru^{II}(bda)(L)_2]$ (H_2bda is 2,2′-bipyridine-6,6′-dicarboxylic acid, HCO_2-bpy-CO_2H; L is isoquinoline, 4-picoline, or phthalazine). They undergo rapid and sustained water oxidation catalysis with added Ce^{IV}. A mechanism has been proposed in which initial oxidation to seven coordinate Ru^{IV} is followed by further oxidation to Ru^V(O) with O–O coupling to give a peroxo-bridged intermediate, $Ru^{IV}O\text{–}ORu^{IV}$, which undergoes further oxidation and release of O_2 (21, 22). We report here the results of a rate and mechanistic study on electrochemical water oxidation by complex [**1**], $[Ru^{II}(CO_2\text{-bpy-}CO_2)(isoq)_2]$ (isoq is isoquinoline) (Fig. 1). Evidence is presented for water oxidation by a chelate open form in acidic solutions. The chelate open form displays dramatic rate enhancements with added buffer bases, and the results of a detailed mechanistic study are reported here.

Results and Discussion

Fig. 2 compares cyclic voltammograms (CVs) for complex [**1**] in 0.1 M $HClO_4$ and at pH 7.0 [0.20 M $H_2PO_4^-/HPO_4^{2-}$ phosphate buffer, I = 0.5 M ($NaClO_4$)] in 4% (vol/vol) CH_3CN at a glassy carbon electrode (GC) (0.071 cm^2). The Ag/AgCl [3 M NaCl, 0.21 V vs. normal hydrogen electrode (NHE)] reference electrode was isolated with an electrolyte filled bridge to avoid chloride ion diffusion into the anode compartment. The sample was purged with argon to remove O_2 before each scan, with only O_2 freshly produced in oxidative scans detected on reverse scans at –0.3 V vs. NHE, a peak potential (E_p) for the O_2/O_2^- couple (5, 23). As shown in Fig. 2, and as reported earlier by Sun and coworkers (21), in 0.1 M $HClO_4$ there is evidence for catalytic water oxidation but electrocatalysis under these conditions is relatively slow. However, significantly enhanced catalytic currents are observed at pH 7.0 with added phosphate buffer and the overpotential for water oxidation is only about 0.2 V. The low overpotential and high reactivity toward water oxidation compared with other Ru polypyridyl water oxidation catalysts is notable. Also notable in the CVs is the appearance at pH 1.0 of evidence for two redox couples before the onset of water oxidation, whereas only one redox couple is observed at pH 7.0 before catalytic water oxidation.

The results of pH-dependent differential pulse voltammetry (DPV) measurements in 4% (vol/vol) CH_3CN are summarized in the E-pH (Pourbaix) diagram in Fig. 3*A*. From the CV data and the diagram, at pH 7.0, $2e^-$ oxidation of Ru^{II} to Ru^{IV} occurs at $E_{1/2}$ = 0.83 V vs. NHE. Although the Ru^{II} complex has been characterized structurally as six-coordinate with the bda ligand tetradentate in the solid state (21), asymmetrical ^1H-NMR and ^{13}C-NMR spectra (*SI Appendix*, Fig. S1) in 1:9 CD_3CN:D_2O (vol/vol) point to a loss of symmetry in solution with terdentate bda coordination, a nonbonded carboxylate arm, and coordinated nitrile, $[Ru^{II}(CO_2\text{-bpy-}CO_2^-)(isoq)_2(NCCH_3)]$. Dissociation of carboxylate group was also found for $[Ru^{II}(bda)(pic)_2]$ (24) and $[Ru^{II}(pda)(pic)_2]$ (25) (H_2pda is 1,10-phenanthroline-2,9-

Significance

Development of rapid, robust water oxidation catalysts remains an essential element in solar water splitting by artificial photosynthesis. We report here dramatic rate enhancements with added buffer bases for a robust Ru(II) polypyridyl catalyst with a calculated half-time for water oxidation of ∼7 μs in 1.0 M phosphate. The results of detailed kinetic studies provide insight into the water oxidation mechanism and an important role for added buffer bases in accelerating water oxidation by concerted atom–proton transfer.

Author contributions: N.S., J.J.C., R.A.B., A.K.V., C.J.D., M.K.C., and T.J.M. designed research; N.S. and R.A.B. performed research; J.J.C., R.A.B., and J.A.R. contributed new reagents/analytic tools; N.S., R.A.B., A.K.V., C.J.D., M.K.C., and T.J.M. analyzed data; and N.S., R.A.B., M.K.C., and T.J.M. wrote the paper.

Reviewers included: R.T., University of Houston.

The authors declare no conflict of interest.

[1]Present address: Chemistry Department, Brookhaven National Laboratory, Upton, NY 11973-5000.

[2]Present address: Department of Chemistry and Biochemistry, University of South Carolina, Columbia, SC 29208.

[3]To whom correspondence should be addressed. Email: tjmeyer@unc.edu.

This article contains supporting information online at www.pnas.org/lookup/suppl/doi:10.1073/pnas.1500245112/-/DCSupplemental.

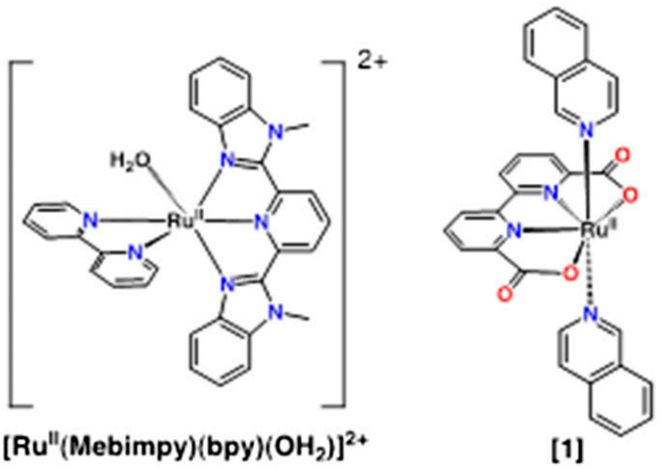

Fig. 1. Structures of $[Ru^{II}(Mebimpy)(bpy)(OH_2)]^{2+}$ (*Left*) and $[Ru^{II}(CO_2\text{-bpy-}CO_2)(isoq)_2]$ [**1**] (*Right*).

dicarboxylic acid) complexes. Terdentate coordination was verified by X-ray crystallography (see below).

However, in 3:1 CD_3OD:D_2O (vol/vol), symmetrical ^{1}H-NMR and ^{13}C-NMR spectra were observed (*SI Appendix*, Fig. S2) consistent with coordination of both carboxylate arms and tetradentate coordination ([**1**] in Fig. 1). A Pourbaix ($E_{1/2}$-pH) diagram in 30% (vol/vol) CF_3CH_2OH–water in the absence of CH_3CN is also shown in Fig. 3*B*. The ∼0.2-V increase in $E_{1/2}(Ru^{III/II})$ with added CH_3CN is notable, consistent with coordination of the nitrile and an increase in $E_{1/2}(Ru^{III/II})$ due to stabilization of Ru^{II} by $d\pi_{Ru}$-π^*(nitrile) back-bonding (26). When oxidized to Ru^{III}, the CH_3CN ligand is readily displaced by H_2O, forming $[Ru^{III}(CO_2\text{-bpy-}CO_2^-)(isoq)_2(OH_2)]^+$, a behavior found in related iron complexes (27). The bound H_2O molecule serves as a proton source when oxidized. Due to the increase in $E_{1/2}(Ru^{III/II})$ with added CH_3CN, the $E_{1/2}$-pH plot for this couple intersects the pH-dependent $Ru^{IV/III}$ couple at pH ∼ 6.0. Past this pH, only the 2e$^-$ $Ru^{IV/II}$ wave is observed and Ru^{III} is either unstable toward disproportionation (10, 11) or undergoes rapid further oxidation.

DPVs in 30% (vol/vol) CF_3CH_2OH at pH 7.0 with added $H_2PO_4^-/HPO_4^{2-}$ buffer and increasing amounts of added CH_3CN are shown in Fig. 4. Waves appear in the DPVs at peak potentials, E_p = 0.64, 0.83, and 0.99 V vs. NHE, for the $Ru^{III/II}$, $Ru^{IV/III}$, and $Ru^{V/IV}$ couples with the current for the latter being significantly enhanced by catalytic water oxidation. With incremental addition of up to 4% (vol/vol) CH_3CN, $E_p(Ru^{III/II})$ at 0.64 V shifts to more positive potentials. With 4% (vol/vol) added CH_3CN, $E_p(Ru^{III/II})$ becomes more positive than $E_p(Ru^{IV/III})$ and a single wave appears for the $Ru^{IV/II}$ couple. In a CV measurement, the integrated area for this wave is consistent with a 2e$^-$ process. E_p for the $Ru^{V/IV}$ couple was unaffected by 4% (vol/vol) added CH_3CN. Forward and reverse DPVs (*SI Appendix*, Fig. S3) were also obtained in 30% (vol/vol) CF_3CH_2OH at pH 7.0 [0.05 M phosphate buffer, I = 0.25 M ($NaClO_4$)], with results consistent with catalytic water oxidation at the onset of the $Ru^{V/IV}$ couple.

The X-ray crystal structure (*SI Appendix*, Fig. S4) of the perchlorate salt reveals a six-coordinate complex with coordinated CH_3CN and a dissociated, protonated carboxylate arm, $[Ru^{II}(CO_2\text{-bpy-}CO_2H)(isoq)_2(NCCH_3)]^+$, consistent with the asymmetric NMR spectra. Evidence for the terdentate ligand complex in solution was also obtained by pH titrations with spectrophotometric monitoring from pH 0.7 to 13.0 (see below).

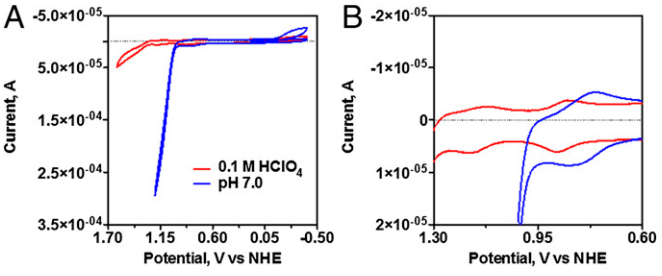

Fig. 2. (*A*) CVs of 0.2 mM [**1**] in 0.1 M $HClO_4$ (red) and at pH 7.0 (blue) 0.20 M $H_2PO_4^-/HPO_4^{2-}$ buffer, I = 0.5 M ($NaClO_4$). GC working electrode, purged with argon before each scan, 4% (vol/vol) added CH_3CN, and scan rate of 100 mV/s. Scan direction: 0 V → −0.39 V → (1.61 or 1.21) V → −0.39 V → 0 V. (*B*) A magnified view of *A* over the potential range 0.60–1.30 V vs. NHE.

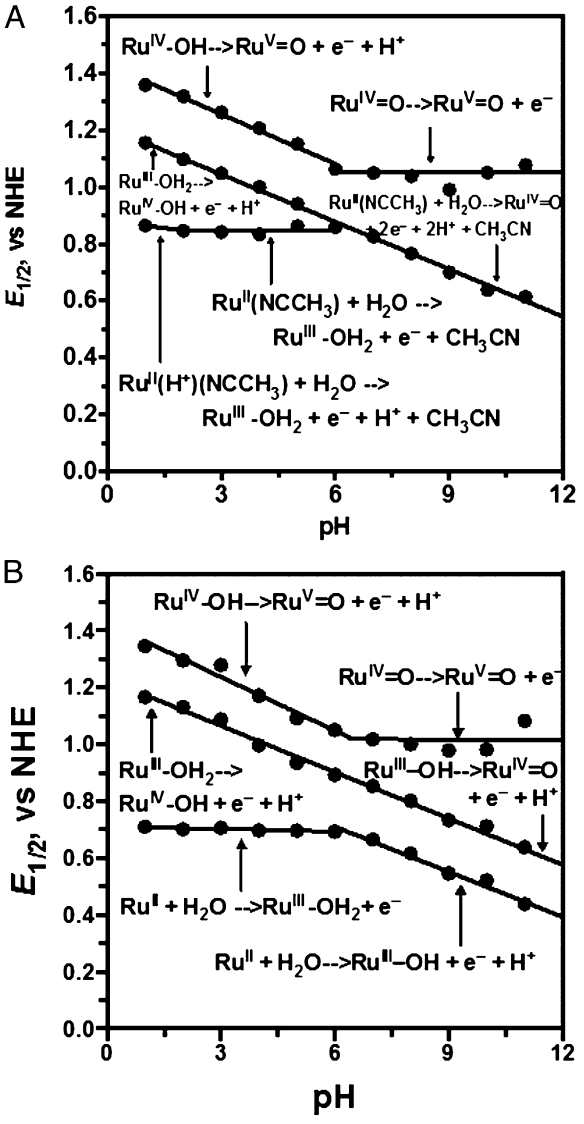

Fig. 3. Pourbaix ($E_{1/2}$-pH) diagram for complex [**1**] in 4% (vol/vol) CH_3CN (*A*) and in 30% (vol/vol) CF_3CH_2OH (*B*) obtained from differential pulse voltammograms (DPVs). $HClO_4$, acetate buffers, phosphate buffers, and borate buffers were used to adjust pH at 0.25 M ionic strength. In *B*, $Ru^{II}(H^+)$ is an abbreviation for $[Ru^{II}(CO_2\text{-bpy-}CO_2H)(isoq)_2(NCCH_3)]$ and Ru^{III}-OH_2 for $[Ru^{III}(CO_2\text{-bpy-}CO_2^-)(isoq)_2(OH_2)]^+$.

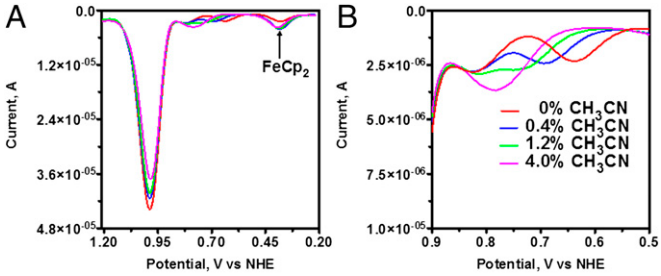

Fig. 4. (*A*) Differential pulse voltammograms (DPVs) with 0.2 mM [**1**] in 30% (vol/vol) CF_3CH_2OH–pH 7.0 [0.05 M phosphate buffer, I = 0.25 M ($NaClO_4$)] mixture with increasing amounts of CH_3CN. Ferrocene ($FeCp_2$) was added as an internal reference. Potential Increment: 4 mV; amplitude: 0.05 V. (*B*) A magnified view of *A* over the potential range 0.50–0.90 V vs. NHE.

Initial titration runs were performed over an extended pH range (0.7–13.0). No significant spectral changes were observed above pH 7 (*SI Appendix*, Fig. S5), except for loss of a very minor impurity absorption (680 nm, $pK_a = 10.8 \pm 0.2$) at high pH.

Subsequent titrations were performed over a limited pH range (0.7–7.2) where protonation of the free and coordinated carboxylate groups of the bda ligand were observed (*SI Appendix*, Fig. S6). Singular value decomposition (SVD) analysis of these data revealed the presence of at least four colorimetric components, requiring a model with three successive pK_a steps. As illustrated in *SI Appendix*, Fig. S6*B*, the process near pH 5.0 produces no significant change in the predicted spectra of colorimetric species **C** and **D**, which suggests that the very small absorbance changes in this pH region simply result from a minor impurity and are not associated with complex [**1**]. The process near pH 2.4 results in small shifts in spectral features and amplitudes, a pK_a value consistent with protonation of the uncoordinated carboxylate group of complex [**1**] identified by X-ray crystallography. The largest change in spectral features occurs in the region below pH 1.5 where protonation and deligation of the remaining carboxylate group is assumed to occur. The titration was not extended to lower pH owing to the likely precipitation of complex [**1**] in concentrated perchloric acid media on the long timescales of the titration experiments. Therefore, the fitting procedure in SPECFIT/32 was constrained with fixed values of $pK_a(1)$. Sensible predicted spectra (positive at all wavelengths) were obtained for $0 \leq pK_a(1) \leq 0.2$. By matching the predicted spectrum of species **A** to that obtained via a pH jump kinetics experiment (see below) a fixed value of $pK_a(1) = 0.2$ was chosen for refinement of the data in *SI Appendix*, Fig. S6.

To assess the reliability of the predicted spectrum of species **A** in *SI Appendix*, Fig. S6*B*, a sample of complex [**1**] in 30% (vol/vol) CH_3CN/H_2O was mixed 1:1 with 30% (vol/vol) CH_3CN/2 M $HClO_4$ (0.7 M acid after mixing), and the spectrophotometric changes were followed for 300 s (*SI Appendix*, Fig. S7). SVD analysis of the spectral data revealed the presence of three colorimetric components, and the data were fit to a kinetic model with two sequential first-order decays ($\mathbf{A} \rightarrow \mathbf{B} \rightarrow \mathbf{C}$): $k_1 = (6.2 \pm 0.2) \times 10^{-2}\ s^{-1}$, $k_2 = (1.8 \pm 0.1) \times 10^{-2}\ s^{-1}$. The fitted spectrum of species **C** in this model corresponds to partial formation (at pH ~0.2) of the extrapolated spectrum predicted by SPECFIT/32 for species **A** in the pH titration experiment (*SI Appendix*, Fig. S6*B*).

Comparison of CVs of [**1**] at different electrodes was conducted at pH 7.0 with GC, fluorine-doped tin oxide (FTO) and FTO electrodes derivatized by surface binding of the electron transfer shuttle $[Ru^{II}(bpy)_2(4,4'\text{-}(PO_3H_2)_2bpy)]^{2+}$ (RuP) (28, 29) (Fig. 5*A*). Higher catalytic currents were observed at GC compared with FTO with no significant current enhancement observed at FTO up to 1.6 V (Fig. 5*B*). An absence of

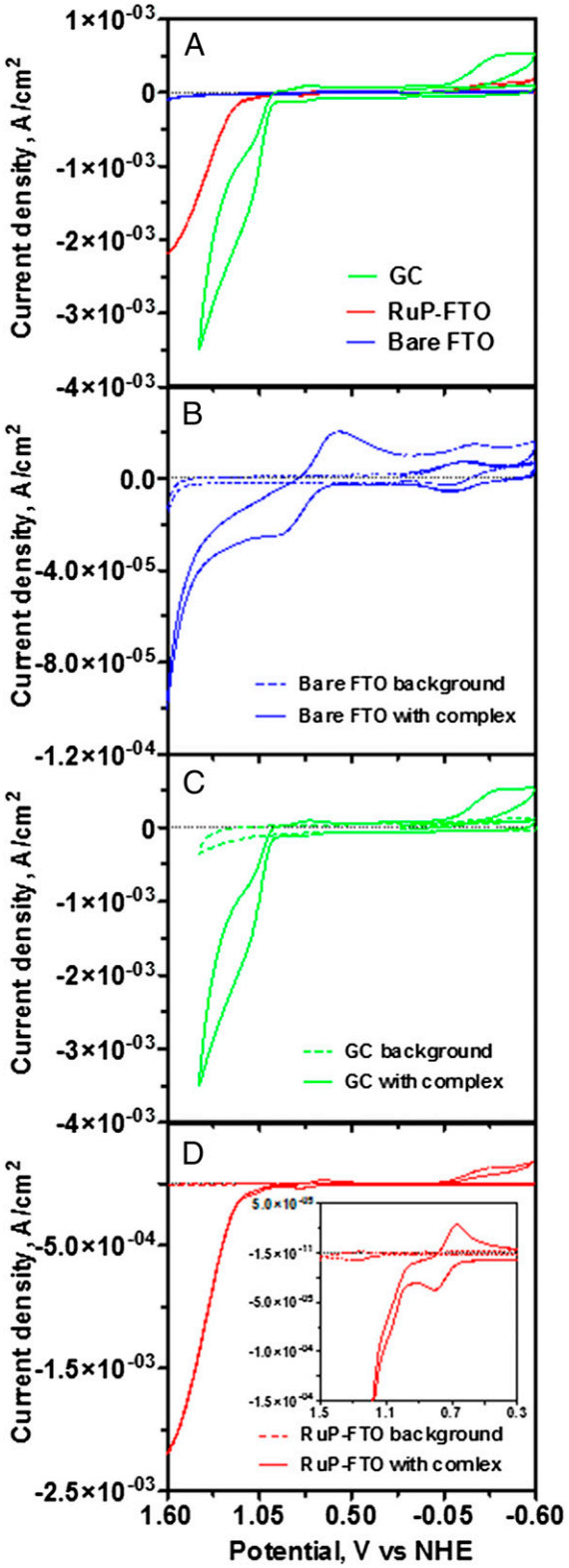

Fig. 5. (*A*) CVs of 0.2 mM complex [**1**] at different electrodes: GC working electrode (green), bare FTO (blue), and RuP-FTO (red). pH 7.0 with 0.10 M phosphate buffer, I = 0.5 M ($NaClO_4$), argon was purged before each scan, 4% (vol/vol) CH_3CN, and scan rate of 100 mV/s. Comparison of background (dashed lines) and in the presence of complex (solid lines) at bare FTO (*B*), GC (*C*), and RuP-FTO (D). The *Inset* in *D* shows an expanded view. RuP is $[Ru(bpy)_2(4,4'\text{-}((HO)_2(O)P)_2\text{-}bpy)]^{2+}$, which is surface attached to FTO and functions as an electron transfer mediator.

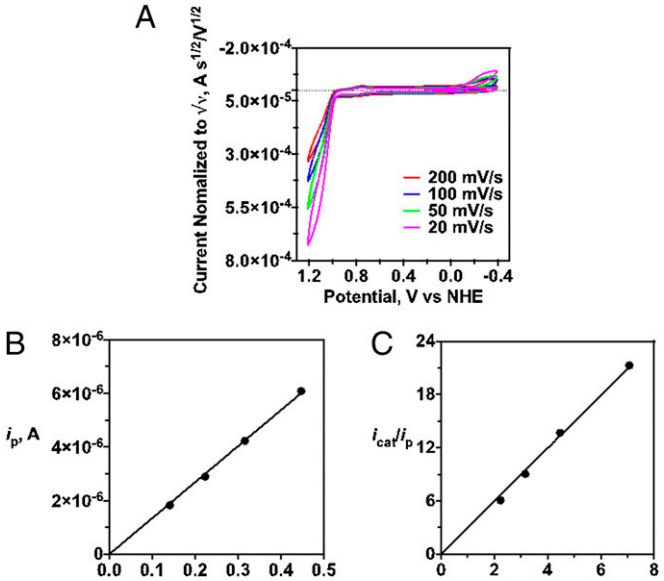

Fig. 6. CV scan rate dependence with 0.2 mM complex [**1**] at pH 7.0 [0.10 M phosphate buffer, I = 0.5 M ($NaClO_4$)], GC working electrode, argon was purged before each scan, 4% (vol/vol) CH_3CN, and scan rate of 20 mV/s (magenta), 50 mV/s (green), 100 mV/s (blue) and 200 mV/s (red). (*A*) CVs with current normalized to the square root of the scan rate. (*B*) Dependence of the peak current (background subtracted) for the Ru(IV/II) couple ($E_{1/2}$ = 0.80 V) on the square root of scan rate. (*C*) Plot of i_{cat}/i_p vs. $1/\upsilon^{1/2}$. i_{cat} was measured at 1.08 V vs. NHE.

electroactivity at oxide electrodes has been reported for neutral organic molecules (30). At FTO electrodes modified by addition of RuP, an electrochemical response for [**1**] is observed including evidence for catalytic water oxidation (Fig. 5*D*).

Scan rate normalized CVs ($i/\upsilon^{1/2}$: υ is the scan rate) from 20 to 200 mV/s at pH 7.0 [0.10 M $H_2PO_4^-/HPO_4^{2-}$ buffer, I = 0.5 M ($NaClO_4$)] in 4% (vol/vol) CH_3CN are shown in Fig. 6*A*. The waveform for the Ru(IV/II) couple at $E_{1/2}$ = 0.80 V is scan rate independent under these conditions. Its peak current (i_p) varies linearly with $\upsilon^{1/2}$ (Fig. 6*B*) consistent with the Randles–Sevcik relation in Eq. **1**, and diffusion-limited electron transfer at the electrode (31). In Eq. **1**, A is the electrode area, F the Faraday, i_p the peak current, [Ru^{II}] the bulk concentration of complex, and n = 2 is the number of electrons transferred. The diffusion coefficient, $D \cong 1.6 \times 10^{-6}$ $cm^2 \cdot s^{-1}$, was obtained from the scan rate dependence of i_p (Fig. 6*B*).

There is clear evidence in the CVs for catalytic water oxidation at higher potentials by the current enhancements that appear following oxidation of Ru^{IV} to Ru^{V} at $E_{p,a}$ = 1.08 V. Peak currents increase with decreasing scan rates consistent with a contribution to the waveform from rate-limiting water oxidation catalysis:

$$i_p = 0.446nFA\left[Ru^{II}\right](nF\upsilon D/RT)^{1/2}, \quad [1]$$

$$i_{cat} = n'FA\left[Ru^{II}\right](Dk_{cat})^{1/2}. \quad [2]$$

CVs of 0.2 mM [**1**] at a glassy carbon electrode with 4% (vol/vol) added CH_3CN were used to explore the role of the added buffer base HPO_4^{2-}. In these experiments, the pH was held constant at 7.0 while the total concentration of buffer, $H_2PO_4^- + HPO_4^{2-}$, was increased. The ionic strength was maintained at I = 0.5 M with added $NaClO_4$. Variations in peak currents for water oxidation at E_p = 1.08 V and O_2 reduction are shown in Fig. 7. At slow scan rates and low buffer concentrations, nearly ideal plateau wave shapes were observed reaching a current maximum at 1.08 V. Reproducible CV measurements further indicate the catalyst is stable following multiple catalytic turnovers.

Rate constants for water oxidation were evaluated from the current ratio i_{cat}/i_p and Eq. **3** assuming a reaction first order in catalyst (see below) (31). In this equation, k_{cat} is the rate constant for the catalyzed reaction with n' = 4 and i_p the peak current for the $Ru^{II} \rightarrow Ru^{IV}$ wave (n = 2). i_{cat} was evaluated at $E_{p,a}$ = 1.08 V, an overpotential of 260 mV for water oxidation at pH 7.0. As shown in Fig. 6*C*, the expected linear variation of i_{cat}/i_p with $\upsilon^{-1/2}$ is observed with k_{cat} calculated from the slope:

$$\frac{i_{cat}}{i_p} = 2.24\frac{n'}{n}\left(\frac{k_{cat}RT}{nF\upsilon}\right)^{1/2} = 0.508\left(\frac{k_{cat}}{\upsilon}\right)^{1/2}. \quad [3]$$

The dependence of the ratio $(i_{cat}/i_p)^2$ (and k_{cat}) on [HPO_4^{2-}] at pH 7.0 in $H_2PO_4^-/HPO_4^{2-}$ buffers from the CV measurements is shown in Fig. 8*A*. It is consistent with the expression in Eq. **4** with $k_{HPO_4^{2-}} = 499 \pm 29$ $M^{-1} \cdot s^{-1}$ from the slope and $k_{H2O} \cong 6$ s^{-1} from the intercept. The term k_{H2O} is the rate constant for unassisted water oxidation. k_B includes contributions from both HPO_4^{2-} and $H_2PO_4^-$ as proton acceptor bases with the former expected to dominate based on earlier results (17) and the increase in pK_a from 2.15 for H_3PO_4 to 7.20 for $H_2PO_4^-$:

$$\left(\frac{i_{cat}}{i_p}\right)^2 = \frac{0.258}{\upsilon}\left(k_{H_2O} + k_B[B]\right). \quad [4]$$

Under the same conditions at pH 7.0 with [**1**] varied from 0.05 to 0.40 mM, i_{cat} at 1.08 V increases linearly with catalyst concentration, *SI Appendix*, Fig. S8. This is in contrast to acidic solutions with Ce^{IV} as the oxidant where a second-order dependence on [**1**] has been reported (21). Under our conditions, with electrochemical monitoring at pH 7.0, the observed behavior is similar to that observed earlier for related single-site Ru polypyridyl catalysts. For these catalysts, oxidation to Ru^{V}=O is followed by rate-limiting O-atom transfer to H_2O (11, 16, 17, 19, 20). Recently, Sun and coworkers (32) reported that the bda-carbene catalyst, [Ru^{III}(bda)(mmi)(OH_2)] (mmi is 1,3-dimethylimidazolium-2-ylidene) undergoes single-site catalytic water oxidation at pH 1.0.

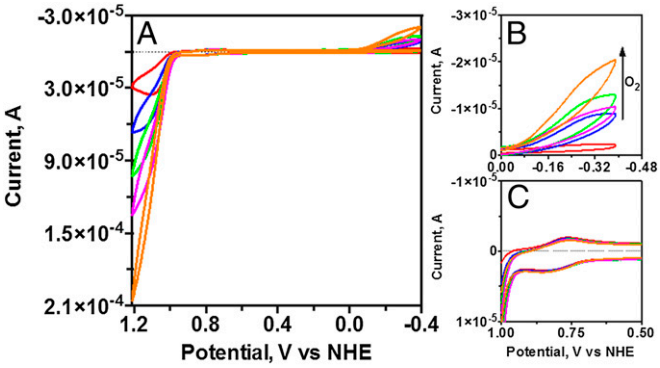

Fig. 7. (*A*) CVs of 0.2 mM [**1**] at pH 7.0 in $H_2PO_4^-/HPO_4^{2-}$ buffers with 4% (vol/vol) CH_3CN and I = 0.5 M ($NaClO_4$). Buffer concentrations are 0.01 M (red), 0.05 M (blue), 0.10 M (green), 0.15 M (magenta), and 0.20 M (orange), GC working electrode, purged with argon before each scan, 4% (vol/vol) added CH_3CN, and scan rate of 20 mV/s. Scan direction: 0 V → −0.39 V → 1.21 V → −0.39 V → 0 V. Magnified views show the O_2 reduction (*B*) and the Ru(IV/II) waves (*C*), respectively.

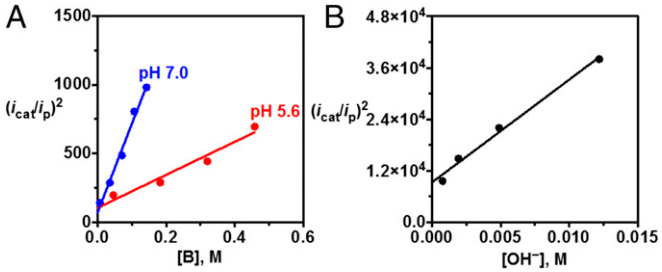

Fig. 8. Plots of k_{obs} vs. buffer base concentration for (*A*) OAc^- in a HOAc/OAc^- buffer at pH 5.6 (red) and with HPO_4^{2-} in a $H_2PO_4^-/HPO_4^{2-}$ buffer at pH 7.0 (blue). [**1**] = 0.2 mM, I = 0.5 M ($NaClO_4$), GC working electrode, 4% (vol/vol) CH_3CN, and scan rate of 20 mV/s with i_{cat} measured at 1.16 V with OAc^- and at 1.08 V for HPO_4^{2-}. (*B*) As in *A*, [OH^-] dependence at pH 11.0–12.2, [PO_4^{3-}] is 36 mM, and scan rate is 100 mV/s with the pH varied from 11.0 to 12.2 by varying [HPO_4^{2-}] in HPO_4^-/PO_4^{3-} buffers with i_{cat} measured at 1.31 V vs. NHE.

Given the evidence from NMR, the X-ray crystal structure, and the results of spectrophotometric titrations with added CH_3CN, the bda complex exists predominantly as $[Ru^{II}(CO_2\text{-bpy-}CO_2H)(isoq)_2(NCCH_3)]^+$ in acidic solutions and as $[Ru^{II}(CO_2\text{-bpy-}CO_2^-)(isoq)_2(NCCH_3)]$ above pH 2.4. It undergoes $2e^-$ oxidation with loss of the nitrile ligand to give Ru^{IV}. Ru^{IV} could be the six-coordinate oxo form, $[Ru^{IV}(CO_2\text{-bpy-}CO_2^-)(isoq)_2(O)]$, or, perhaps, seven-coordinate $[Ru^{IV}(CO_2\text{-bpy-}CO_2)(isoq)_2(OH)]^+$ with the carboxylate arm recoordinated.

Base catalysis with acetate as the added base was investigated at pH 5.6 with 0.05–0.50 M added buffer at I = 0.5 M ($NaClO_4$). CVs are shown in *SI Appendix*, Fig. S9, with i_{cat} values measured at 1.16 V vs. NHE, an overpotential for water oxidation of 260 mV at this pH. From the plot of $(i_{cat}/i_p)^2$ vs. [OAc^-] in Fig. 8*A*, k_{OAc-} = 93 ± 14 $M^{-1}\cdot s^{-1}$ and $k_{H2O} \cong 6\ s^{-1}$ with the latter consistent with the value obtained from the measurements with added $H_2PO_4^-/HPO_4^{2-}$ buffer.

H_2O/D_2O kinetic isotope effects (KIEs) were investigated with added 0.32 M OAc^- (pH 5.6 or 0.32 M d^3-OAc^- at pD 6.2) and 0.071 M HPO_4^{2-} (pH 7.0 or 0.071 M DPO_4^{2-} at pD 7.6). Under these conditions, i_{cat}^2 decreases linearly with the mole fraction of D_2O, as shown in *SI Appendix*, Fig. S10. From these data, KIEs [$=k_{cat,H2O}/k_{cat,D2O}$ from the ratio $(i_{cat,H2O}/i_{cat,D2O})^2$] of 2.6 for acetate and 1.4 for HPO_4^{2-} were obtained, respectively. These results are consistent with a concerted pathway in the rate-limiting step, with the magnitude of the KIE dependent on the basicity of the acceptor base and the symmetry of the preformed H-bond (33).

A dependence on [OH^-] was also investigated by rate measurements with [PO_4^{3-}] = 36 mM by varying the buffer ratio from pH 11.0 to 12.2 [I = 0.5 M ($NaClO_4$)]. Results are shown in *SI Appendix*, Fig. S11. From the slope of a plot of $(i_{cat}/i_p)^2$ vs. [OH^-] (Fig. 8*B*), k_{OH-} = (9.3 ± 0.6) × 10^5 $M^{-1}\cdot s^{-1}$ with an intercept = (3.6 ± 0.4) × 10^3 $s^{-1} \cong k_{PO_4^{3-}} \times [PO_4^{3-}]$. From the latter, $k_{PO_4^{3-}} \cong$ (1.0 ± 0.1) × 10^5 $M^{-1}\cdot s^{-1}$.

The considerable rate enhancements with added buffer bases and OH^- are summarized in Table 1. As reported earlier for other single-site, polypyridyl $Ru^V(O)$ oxidants with added buffer bases (17, 20), the rate law is consistent with rate-limiting O-atom transfer from $Ru^V(O)$ to a water molecule with O–O bond formation. In this interpretation, O–O bond formation is dominated by APT with proton transfer occurring to added proton acceptor bases as illustrated for HPO_4^{2-} in Eq. **5** (17). Once formed, the hydroperoxide intermediate undergoes further oxidation at the electrode and O_2 release, Eq. **6**, to complete the catalytic cycle (11, 16, 17, 19, 20). The notable rate acceleration with added OH^- may occur due to OH^- acting as the acceptor base or due to direct OH^- attack on $Ru^V(O)$ to give the intermediate hydroperoxide, Eq. **7** (20).

Table 1. Kinetic data for base-assisted water oxidation at I = 0.5 M ($NaClO_4$) in 4% (vol/vol) CH_3CN at 22 ± 2 °C

B	pK_a, HB	k_B, $M^{-1}\cdot s^{-1}$
H_2O	−1.74	$k_{H2O} \cong 6\ s^{-1}$
OAc^-	4.76	93 ± 14
HPO_4^{2-}	7.20	499 ± 29
PO_4^{3-}	12.35	≅(1.0 ± 0.1) × 10^5
OH^-	15.75	(9.3 ± 0.6) × 10^5

$$[Ru^V(O)]^+ + \text{H-O-H---OP(O)}_2\text{OH}^{2-} \rightarrow [Ru^{III}\text{-OOH}] + \text{HOP(O)}_2\text{OH}^-, \quad [5]$$

$$[Ru^{III}\text{-OOH}] \xrightarrow{-4e^-,\ +H_2O,\ -3H^+} [Ru^V(O)]^+ + O_2, \quad [6]$$

$$[Ru^V(O)]^+ + OH^- \rightarrow [Ru^{III}\text{-OOH}]. \quad [7]$$

Under our conditions, there is no evidence for second-order kinetics and rate-limiting O–O bond formation by $Ru^V(O)$ as found earlier in acidic solution for the picoline derivative (21). However, we cannot rule out a mechanism involving rate-limiting oxidation of Ru^{IV}-OH, presumably as $[Ru^{IV}(CO_2\text{-bpy-}CO_2)(isoq)_2(OH)]^+$, to $[Ru^V(O)]^+$, Eq. **8**, followed by $[Ru^V{=}O]^+$—$[O{=}Ru^V]^+$ coupling. In this interpretation, kinetic enhancements by added proton bases, including OH^-, arise by a proton-coupled electron transfer (PCET) effect with electron transfer to the electrode occurring in concert with proton transfer to the added base by concerted electron–proton transfer (33–37). Note Eq. **8** with HPO_4^{2-} as the proton acceptor base:

$$[Ru^{IV}\text{-OH}]^+ + HPO_4^{2-} \rightleftharpoons Ru^{IV}\text{-O-H}^+\text{---OP(O)}_2\text{OH}^{2-}$$
$$Ru^{IV}\text{-O-H}^+\text{---OP(O)}_2\text{OH}^{2-} \xrightarrow{-e^-} [Ru^V(O)]^+ + [\text{H-OP(O)}_2\text{OH}]^- \text{ (rate limiting)}, \quad [8]$$

$$2[Ru^V{=}O]^+ \rightarrow [Ru^{IV}\text{O-O}Ru^{IV}]^{2+} \quad \text{(rapid)}. \quad [9]$$

Our results demonstrate dramatic rate enhancements in water oxidation by [**1**] with added OAc^-, HPO_4^{2-}, PO_4^{3-}, and OH^-. In a buffer solution, 1.0 M in HPO_4^{2-} at pH 7.2, the rate acceleration for water oxidation is 83-fold compared with pH 1 and 10-fold compared with $[Ru^{II}(Mebimpy)(bpy)(OH_2)]^{2+}$ at pH 7.2 (17). In 1.0 M PO_4^{3-}, the estimated half-time for water oxidation is ~ 7 μs.

Until at high pH with appreciable concentrations of OH^- in solution, pH plays an indirect role with rate enhancements dictated by the concentration of added buffer base and the buffer pK_a. The key to rate accelerations under these conditions is direct involvement of the buffer base in either APT or PCET pathways.

Materials and Methods

All commercial chemical reagents were used as received except as noted. Electrochemical measurements were performed with a CH Instruments CH-660D electrochemical workstation at room temperature. A three-electrode configuration was applied in a single compartment cell with a glassy carbon working electrode, Ag/AgCl reference electrode, and platinum wire counter electrode. Solutions were purged with argon through a solvent bubbler filled with Milli-Q H_2O in order to exclude O_2, reduce evaporation, and to prevent catalyst decomposition. More detailed experimental considerations are provided in *SI Appendix*.

ACKNOWLEDGMENTS. This research was primarily supported by the University of North Carolina Energy Frontier Research Center: Center for Solar

Fuels, an Energy Frontier Research Center funded by the US Department of Energy, Office of Science, Office of Basic Energy Sciences, under Award DE-SC0001011, supporting J.J.C., R.A.B., A.K.V., and M.K.C. The National Science Foundation is acknowledged for supporting N.S. under Grant CHE-0957215. The Swiss National Science Foundation is acknowledged for supporting J.A.R. with an individual Early Postdoc Mobility Fellowship.

1. Neudeck S, et al. (2014) New powerful and oxidatively rugged dinuclear Ru water oxidation catalyst: Control of mechanistic pathways by tailored ligand design. *J Am Chem Soc* 136(1):24–27.
2. Wasylenko DJ, Palmer RD, Berlinguette CP (2013) Homogeneous water oxidation catalysts containing a single metal site. *Chem Commun (Camb)* 49(3):218–227.
3. Hintermair U, et al. (2013) Precursor transformation during molecular oxidation catalysis with organometallic iridium complexes. *J Am Chem Soc* 135(29):10837–10851.
4. Kaveevivitchai N, et al. (2013) A Ru(II) bis-terpyridine-like complex that catalyzes water oxidation: The influence of steric strain. *Inorg Chem* 52(18):10615–10622.
5. Barnett SM, Goldberg KI, Mayer JM (2012) A soluble copper-bipyridine water-oxidation electrocatalyst. *Nat Chem* 4(6):498–502.
6. Kanan MW, Nocera DG (2008) In situ formation of an oxygen-evolving catalyst in neutral water containing phosphate and Co^{2+}. *Science* 321(5892):1072–1075.
7. Ellis WC, McDaniel ND, Bernhard S, Collins TJ (2010) Fast water oxidation using iron. *J Am Chem Soc* 132(32):10990–10991.
8. Mallouk TE (2013) Water electrolysis: Divide and conquer. *Nat Chem* 5(5):362–363.
9. Wang D, Groves JT (2013) Efficient water oxidation catalyzed by homogeneous cationic cobalt porphyrins with critical roles for the buffer base. *Proc Natl Acad Sci USA* 110(39):15579–15584.
10. Concepcion JJ, Jurss JW, Templeton JL, Meyer TJ (2008) One site is enough. Catalytic water oxidation by $[Ru(tpy)(bpm)(OH_2)]^{2+}$ and $[Ru(tpy)(bpz)(OH_2)]^{2+}$. *J Am Chem Soc* 130(49):16462–16463.
11. Concepcion JJ, Tsai MK, Muckerman JT, Meyer TJ (2010) Mechanism of water oxidation by single-site ruthenium complex catalysts. *J Am Chem Soc* 132(5):1545–1557.
12. Badiei YM, et al. (2013) Water oxidation with mononuclear ruthenium(II) polypyridine complexes involving a direct Ru(IV)═O pathway in neutral and alkaline media. *Inorg Chem* 52(15):8845–8850.
13. Wasylenko DJ, Ganesamoorthy C, Koivisto BD, Henderson MA, Berlinguette CP (2010) Insight into water oxidation by mononuclear polypyridyl Ru catalysts. *Inorg Chem* 49(5):2202–2209.
14. Angeles-Boza AM, et al. (2014) Competitive oxygen-18 kinetic isotope effects expose O-O bond formation in water oxidation catalysis by monomeric and dimeric ruthenium complexes. *Chem Sci* 5(3):1141–1152.
15. Murakami M, et al. (2011) Catalytic mechanism of water oxidation with single-site ruthenium-heteropolytungstate complexes. *J Am Chem Soc* 133(30):11605–11613.
16. Chen Z, Concepcion JJ, Meyer TJ (2011) Rapid catalytic water oxidation by a single site, Ru carbene catalyst. *Dalton Trans* 40(15):3789–3792.
17. Chen Z, et al. (2010) Concerted O atom-proton transfer in the O-O bond forming step in water oxidation. *Proc Natl Acad Sci USA* 107(16):7225–7229.
18. Lin X, et al. (2012) Theoretical study of catalytic mechanism for single-site water oxidation process. *Proc Natl Acad Sci USA* 109(39):15669–15672.
19. Chen Z, Concepcion JJ, Hull JF, Hoertz PG, Meyer TJ (2010) Catalytic water oxidation on derivatized nanoITO. *Dalton Trans* 39(30):6950–6952.
20. Vannucci AK, et al. (2013) Crossing the divide between homogeneous and heterogeneous catalysis in water oxidation. *Proc Natl Acad Sci USA* 110(52):20918–20922.
21. Duan L, et al. (2012) A molecular ruthenium catalyst with water-oxidation activity comparable to that of photosystem II. *Nat Chem* 4(5):418–423.
22. Duan L, Araujo CM, Ahlquist MSG, Sun L (2012) Highly efficient and robust molecular ruthenium catalysts for water oxidation. *Proc Natl Acad Sci USA* 109(39):15584–15588.
23. Yeager E (1984) Electrocatalysts for O_2 reduction. *Electrochim Acta* 29(11):1527–1537.
24. Duan L, et al. (2013) Insights into Ru-based molecular water oxidation catalysts: Electronic and noncovalent-interaction effects on their catalytic activities. *Inorg Chem* 52(14):7844–7852.
25. Tong L, Duan L, Xu Y, Privalov T, Sun L (2011) Structural modifications of mononuclear ruthenium complexes: A combined experimental and theoretical study on the kinetics of ruthenium-catalyzed water oxidation. *Angew Chem Int Ed Engl* 50(2): 445–449.
26. Miessler GL, Fischer PJ, Tarr DA (2013) *Inorganic Chemistry* (Prentice Hall, Upper Saddle River, NJ), 5th Ed.
27. Draksharapu A, et al. (2012) Ligand exchange and spin state equilibria of Fe(II)(N4Py) and related complexes in aqueous media. *Inorg Chem* 51(2):900–913.
28. Jurss JW, Concepcion JC, Norris MR, Templeton JL, Meyer TJ (2010) Surface catalysis of water oxidation by the blue ruthenium dimer. *Inorg Chem* 49(9):3980–3982.
29. Hanson K, et al. (2012) Structure-property relationships in phosphonate-derivatized, Ru-II polypyridyl dyes on metal oxide surfaces in an aqueous environment. *J Phys Chem C* 116(28):14837–14847.
30. Gagliardi CJ, Jurss JW, Thorp HH, Meyer TJ (2011) Surface activation of electrocatalysis at oxide electrodes. Concerted electron-proton transfer. *Inorg Chem* 50(6):2076–2078.
31. Zanello P; Royal Society of Chemistry (Great Britain) (2003) *Inorganic Electrochemistry: Theory, Practice and Applications* (Royal Society of Chemistry, Cambridge, UK).
32. Staehle R, et al. (2014) Water oxidation catalyzed by mononuclear ruthenium complexes with a 2,2′-bipyridine-6,6′-dicarboxylate (bda) ligand: How ligand environment influences the catalytic behavior. *Inorg Chem* 53(3):1307–1319.
33. Weinberg DR, et al. (2012) Proton-coupled electron transfer. *Chem Rev* 112(7): 4016–4093.
34. Huynh MHV, Meyer TJ (2007) Proton-coupled electron transfer. *Chem Rev* 107(11): 5004–5064.
35. Fecenko CJ, Meyer TJ, Thorp HH (2006) Electrocatalytic oxidation of tyrosine by parallel rate-limiting proton transfer and multisite electron-proton transfer. *J Am Chem Soc* 128(34):11020–11021.
36. Gagliardi CJ, Vannucci AK, Concepcion JJ, Chen Z, Meyer TJ (2012) The role of proton coupled electron transfer in water oxidation. *Energy Environ Sci* 5(7):7704–7717.
37. Bonin J, Costentin C, Robert M, Routier M, Savéant JM (2013) Proton-coupled electron transfers: pH-dependent driving forces? Fundamentals and artifacts. *J Am Chem Soc* 135(38):14359–14366.